2022 WJTA Conference and Expo
November 2-3 ● New Orleans, Louisiana

Paper

Erosion of an Air-injected Plain Waterjet (iPWJ)

J. Poloprudský
Institute of Physics of Materials, CAS,
Brno, Czech Republic

M. Schüler, T. Bergs
Fraunhofer Institute for Production Technology IPT
Aachen, Germany

ABSTRACT

The article describes the fundamental characteristics of a plain waterjet (PWJ) tool enhanced by air. An injection-type abrasive waterjet (AWJ) head was used, in which the entrained abrasive was replaced by a defined air input. A two-phase PWJ was created by the injection principle (iPWJ). In dependence on the air pressure supplied, the footprint of the perceived jet tool was characterized. A standard aluminum alloy EN AW-5083 was chosen for the material to be machined. The experiments were designed with two water pressure levels, and four pressure conditions of the air inlet that varied from blocked air, atmospheric conditions, and overpressure. An evaluation was conducted for the visual shape of the free jet and the perceived erosion characteristics of the specimen by scanning electron microscopy (SEM).

1. Introduction

The demand for improvements in the application of waterjet machining has increased in recent years. Plain Waterjet (PWJ) machining still offers some advantages for special applications over its abrasive-enhanced counterpart [1]. However, both the effectiveness of the PWJ and the quality of the surfaces machined were of great significance in recent years. A major route was the optimization of the jet tool by modulating or pulsating waterjet [2], high-pressure pumps, or cryogenic jets [3] to overcome the use of abrasives. High effort on the system side and the related costs of the machine systems are common problems for all approaches. Therefore, a high-adaptive and more accessible approach was proposed to encourage industrial acceptance and meet the needs of small and medium enterprises [4]. A simple but innovative approach to changing the erosion characteristics of a PWJ is presented here by adapting a standard abrasive waterjet (AWJ) tool to be used with pressurized air instead of entraining abrasives.

2. State of the Art

PWJ, as the systematically simplest form of a waterjet, just squeezes pressurized water through an orifice. If solid particles or abrasives are added to the waterjet, this is generally referred to as an abrasive waterjet. Abrasive waterjet variants can be subdivided according to the type and location of the abrasive supply. If the abrasive is fed through an injector system, this standard in the industry is referred to as an injection-type Abrasive Waterjet (AWJ), which is the system currently predominantly used in manufacturing. Opposite, a previously mixed suspension of water and solids is referred to as an Abrasive Suspension Jet (ASJ), which is currently used for special applications or reconstruction but has not been established in production scenarios yet.

The choice of the waterjet mode is typically given by its application. PWJ is typically used for the processing of relatively soft or sensitive materials. AWJ enables the processing of virtually all materials and represents an extension of the PWJ on the system side by adding a mixing unit to the device. Due to the Venturi effect, the high velocity of the PWJ creates a local vacuum in the mixing chamber, which sucks an airstream that is used to transport the added particles and inject them into the mixing chamber. The kinetic energy of the pure waterjet is then used to accelerate the added particles and to shape the composing jet through the focus tube. The resulting jet tool consists of water, abrasive, and air that all expand to fill the inner diameter of the focus tube. This is contrary to the ASJ where both water and abrasive are accelerated simultaneously through a nozzle, typically giving better efficiency. The construction of an ASJ tool is very similar to that of a PWJ, with the nozzle as the essential wear part. Categorization can be done based on the phase composition of waterjet variants (**Figure 1**):

- one-phase PWJ (water)
- two-phase ASJ (water + abrasives)
- two-phase iPWJ (water + air)
- three-phase AWJ (water + abrasives + air)

A PWJ, containing just water, consists of a single-phase fluid. A two-phase abrasive jet can be generated by added solids (ASJ). The absence of an air phase is promising for higher cutting performance with better efficiency and intensity. [5]. A newly introduced two-phase injection plain waterjet (iPWJ) is based on a regular injection AWJ head without adding abrasives to

present an air-enhanced PWJ tool. As a note, the aim can be considered contrary to waterjet cutting, where kinetic intensity is key. However, the industrial standard for abrasive waterjet cutting is still a three-phase AWJ [6].

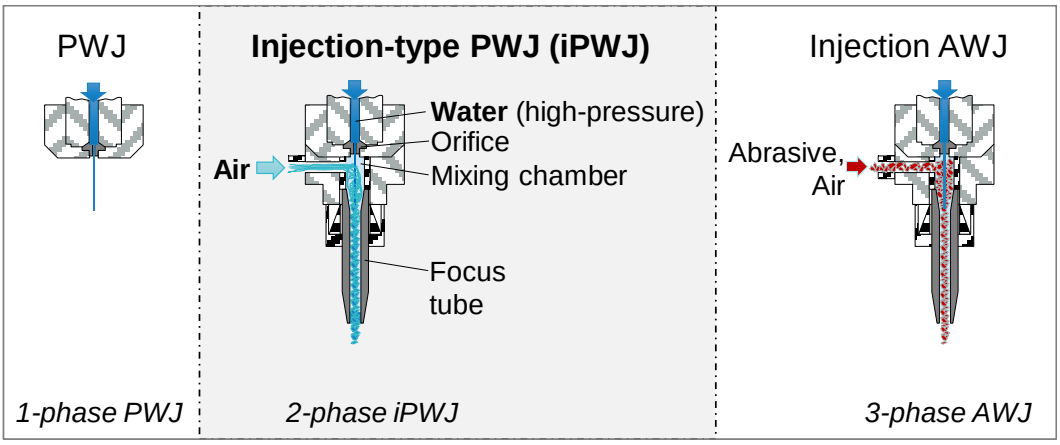

Figure 1. Schematic of an iPWJ configuration

When it comes to AWJ, the acceleration of the abrasive particles by the initial PWJ down the focus tube leads to subsequent surface contacts and wear, accompanied by a lower overall velocity. Due to interactions with the high air content within the jet, a turbulent waterjet is created. According to the injection principle, the main energy transfer takes place behind the mixing chamber. Here, the inner surfaces of the focus tube are intensively stressed during an unsteady acceleration process. The expansion of the jet, the presence of a considerable amount of air, and the overall lower efficiency of this mixing process must be compensated. For example, a higher system pressure leads to increased wear of the orifice or other high-pressure components and the pump itself. In earlier studies, the gaseous and compressible phase of entrained air was neglected. It should be noted that an injection AWJ consists of up to 95 % volume of air. Later studies considered this complex phenomenon fundamentally [7-8]. Several methods were considered, such as finite element simulation, jet visualization, high-speed imaging, pressure profile parameters, or empiric studies [9]. However, the body of research mainly consists of parametric studies combined with jet visualization.

Huang et al. [10] modeled a velocity field inside the injection head using computational fluid dynamics (CFD). The results showed that the highest waterjet velocity was achieved directly behind the entrance into the mixing chamber and slowly decelerates with increasing distance from it, developing a regular flow pattern. Osman et al. [7] analyzed a two-phase flow in a focus tube of a typical diameter under varying waterjet velocities, as well as varying nozzle and mixing tube diameter ratios. The airflow in the study was either restricted completely by blocking the air inlet or allowing free atmospheric flow. The analysis was approached in two main steps. The first step was a static visualization of the waterjet structure at the focus tube entry and downstream towards the nozzle. The second step of the analysis was based on static pressure measurements down the focus tube. In the case of the free atmospheric airflow, the pressure distribution along the focus tube follows a similar trend for all water velocity levels only differing in the resulting jet velocity and proportions of the pressure-affected areas. The first observed area in the focusing tube was the expansion region where a significant decrease in local pressure was observed. The negative pressure gradient in this region was related to air acceleration. The second area inside the focus tube was considered the region of constant pressure. In this region, the airflow reached a roughly uniform state. The third area, called a recompression region, was where the local pressure rapidly changes to the atmospheric

condition. The size of this area was dependent on the jet velocity v_{Jet}. For lower jet velocities $v_{Jet} < 447\ \mathrm{m/s}$, the recompression zone was spread out over the jet length. In the case of high velocities $v_{Jet} > 447\ \mathrm{m/s}$ the recompression region was located at the nozzle. In the case of blocked air suction, the recompression zone for low jet velocities and small jet diameters occurred gradually along the length of the focus tube. For blocked air suction, in combination with high jet velocities and large jet diameters, the pressure development in the focus tube consists of two areas. The first region was of constant pressure, which approaches vapor saturation pressure. The second region was a recompression region with a high-pressure gradient that was concentrated close to the focus tube exit [7].

Himmelreich [11] divided the phenomena inside the focus tube into two categories based on the ratio of the inner diameter of the focus tube to the inner diameter of the orifice ($\emptyset d_F/\emptyset d_O$). In the case of $\emptyset d_F/\emptyset d_O$ = 2.75, Himmelreich observed pipe flow in the focus tube. A free waterjet was observed in the focus tube with a higher ratio of $\emptyset d_F/\emptyset d_O$ = 4. Transferred, this means that for small diameter ratios $\emptyset d_F/\emptyset d_O$ the air was compressed while in larger ratios $\emptyset d_F/\emptyset d_O$ the entrained air was accelerated by the jet.

Momber [9] focused on the processes inside the mixing chamber approaching from an energetic point. An energy transfer from the high-speed water to the solid particles was described, which are introduced into the mixing chamber at a relatively low speed. Due to the lower pressure inside the chamber, the air was sucked into the mixing chamber. During this energy transfer process of the involved phases, the primary waterjet decelerates to generate the exiting multi-phase jet of water, abrasive, and air combined.

In the recent work of Bergs et al. [12], it was seen that the interaction of various phases occurs at several levels. The injection principle introduces some phenomena that alter the machining results. The researchers primarily compared the resulting surfaces of quenched and annealed 42CrMo4 either with AWJ or ASJ. Both were then post-treated using a two-phase iPWJ. The Interaction of the involved jet phases revealed fundamental effects of the gaseous phase within the machining results. Nevertheless, the proceedings of their work [13] proposed a great potential for multi-stage machining.

Even though the mass flow of the sucked air is very small compared to the mass flow of the other phases of an AWJ, the influence of the air phase and its comparative huge volume has been neglected in the past. However, the role of the air phase and its importance for process understanding is still lacking. The volume of entrained air has significant effects on the shape and stability of the jet when it exits the tool head [7].

3. Methodology

The effect of entrained air on the characteristics of an iPWJ tool and its effect on material erosion were not investigated yet. Consequently, this study uses a modified iPWJ configuration and enhances inlet conditions. Here, the inlet port was hermetically modified to create different conditions, for example by pressurization. The experiment concentrated on the erosion characteristics of the modified iPWJ tool onto an aluminum specimen. By varying both the water pressure (p_W) and the pressure of supplied air (p_A), the ratio of the phase composition, and thus its effect on the waterjet tool, were investigated. A comparison was made between the footprint at a water pressure level of $p_W = 200$ MPa and $p_W = 400$ MPa, respectively. Accordingly, the airflow into the mixing chamber was controlled at the abrasive inlet. The air

pressure ranged from a blocked inlet $p_A\,(0)$, through atmospheric conditions at the inlet $p_A\,(0) = 1000\,hPa$ up to pressurization of $p_A\,(2) = 2000\,hPa$ and $p_A\,(3) = 3000\,hPa$, respectively. The main variable to be observed was the airflow introduced into the mixing chamber. Here, the airflow was set by a mechanical pressure regulator and checked with a mechanical flow meter (**Figure 2**). A preliminary study was conducted to choose a constant feed rate $v_F = 2000\,mm/min$ in combination with a standoff distance (SOD) between the surface of the specimen and the nozzle of the focus tube at two levels: SOD = 4 mm and SOD = 54 mm. The jets with given parametric variations according to **Table 1** were then applied to the aluminum specimen. The footprints were then studied visually to understand the effect of air conditions on the tool characteristics by its shape and erosion effects.

Table 1. Factors and levels of the experiments

Material of the specimen	Water Pressure p_W [MPa]	Standoff Distance SOD [mm]	Air Pressure p_A [MPa]	Feed rate v_F [mm/s]	Orifice Diameter $\emptyset d_O$ [mm]	Focus Tube Diameter $\emptyset d_F$ [mm]
AW 5083	200 - 400	4; 54	0 - 0.3	2000	0.20	0.76

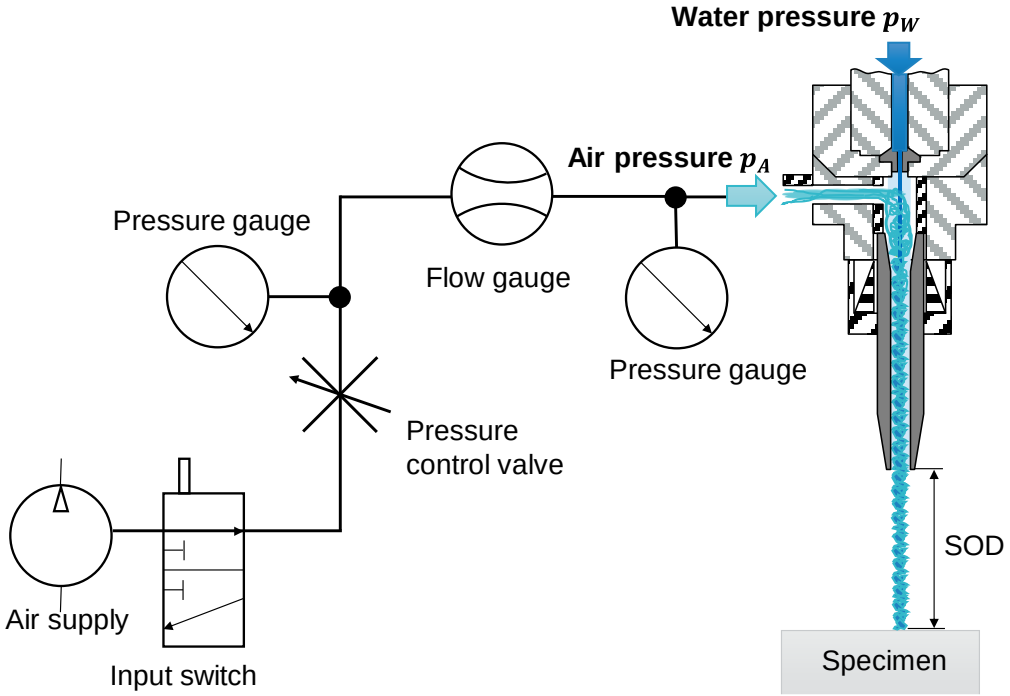

Figure 2. Schematics of the experimental device

The geometry of grooves was measured with the digital microscope Olympus DSX1000 while the microstructure of the material was observed by scanning electron microscope (SEM). A Zeiss type Neon 40 EsB and a Tescan LYRA 3 XMH FEG/SEM were used here. For the free jet analysis, a Nikon type D850 digital camera combined with a 60 mm macro lens was used and the images were processed with ImageJ software.

The experiments were carried out on a customized 5-axis waterjet machine H.G. Ridder type E, equipped with a pressure intensifier pump capable of pressures up to 400 MPa. A standard injection head was used for the experiments, equipped with a 0.20 mm orifice in combination with a 0.76 mm focus tube. The abrasive inlet was used to control the air-flow input. The airflow at different levels of water pressure p_W were measured for different levels of air pressure p_A as shown in **Figure 3** a). For comparison, the suction pressure of a blocked inlet into the mixing chamber over the applied levels of water pressure p_W is shown in **Figure 3** b).

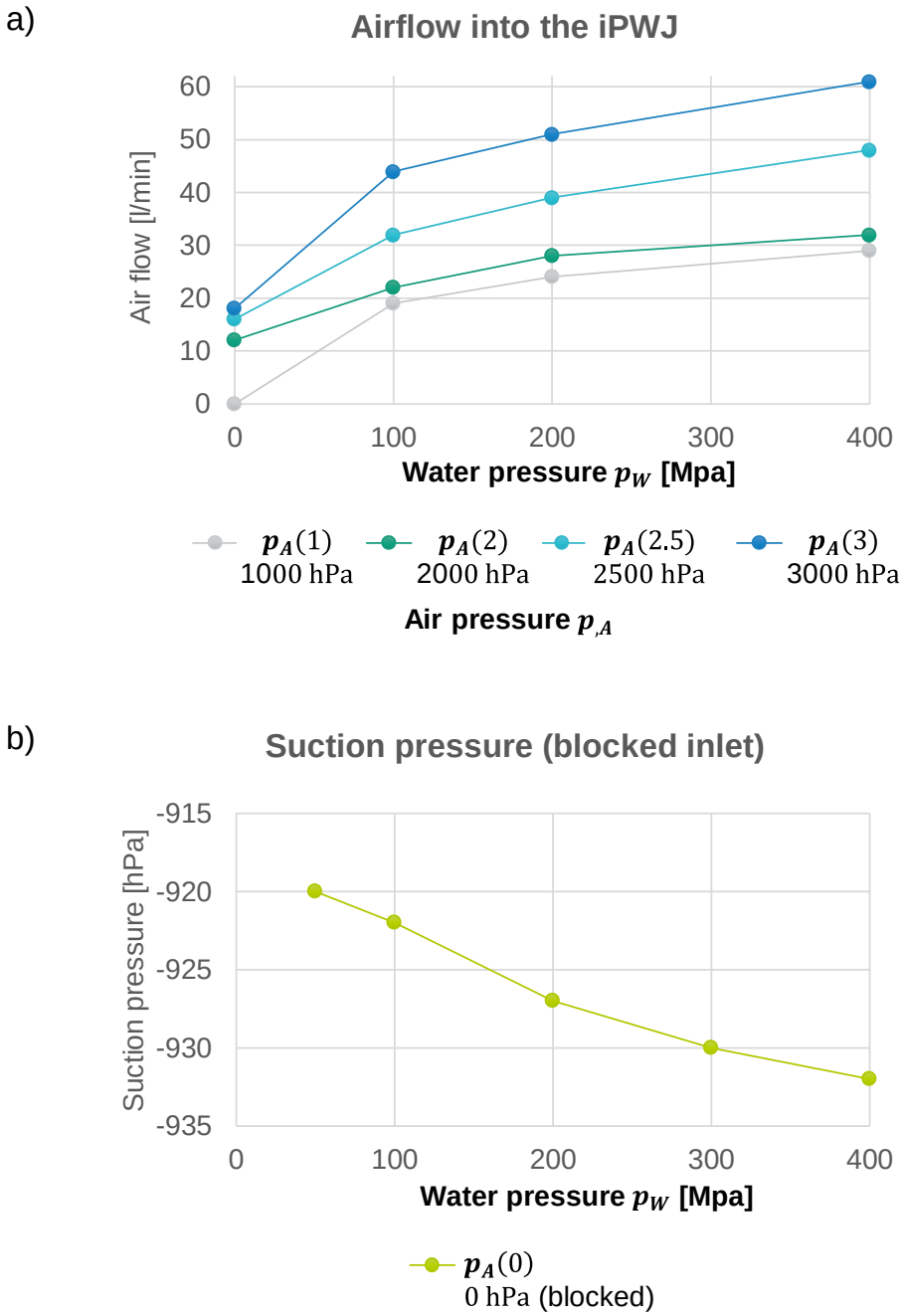

Figure 3. a) Measured airflow $\dot{V}_A$ over the waterjet pressure p_W at several air pressure levels p_A b) Suction pressure inside the mixing chamber for the investigated levels of water pressure p_W.

A wrought aluminum alloy EN AW-5083 with magnesium and manganese as the basic alloying elements was polished and prepared as a specimen. **Table 2** gives the composition measured by Energy dispersion spectroscopy (EDS). The main constituent particles observed in material

matrices are MnFe and MgSi, as documented in **Figure 4**, elongated and uniformly distributed in the material.

Table 2. Alloy composition as measured by EDS

Element	Al	Mg	Mn	Fe	Si
Weight %	94.19	5.07	0.5	0.14	0.11

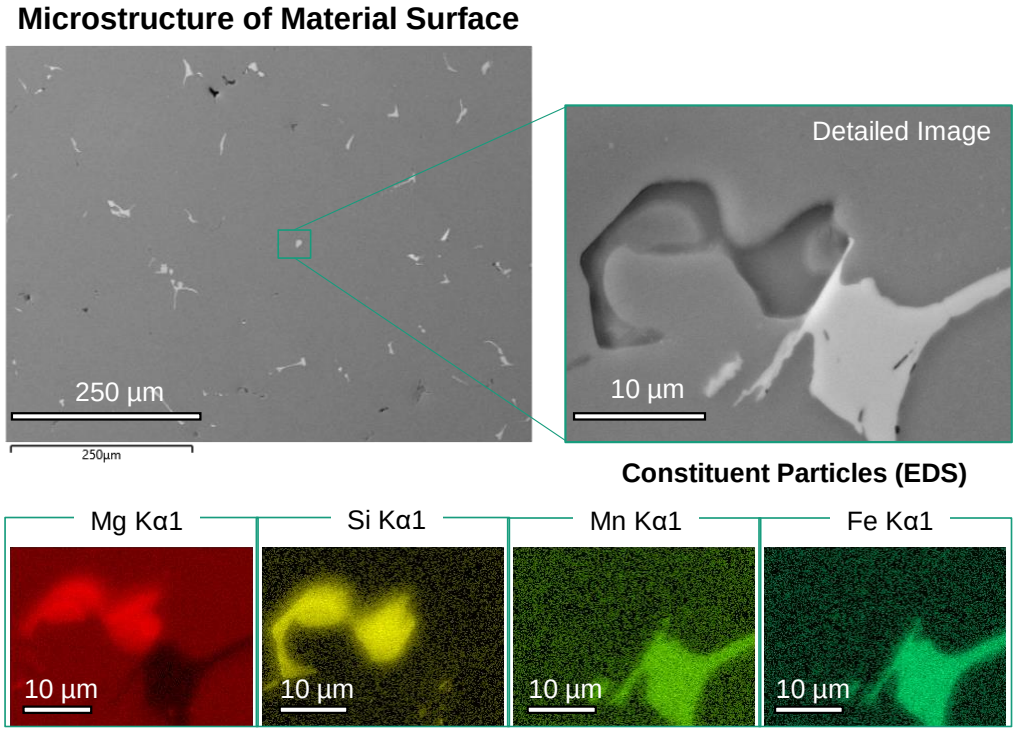

Figure 4. Microstructure of experimental material and EDS analysis of the constituent particles

4. Results and Discussion

Jet shape

In the first part, the airflow for different levels of both air pressure p_A and water input pressure p_W was measured. Then the visualization of the resulting shape of the free jet was presented. In the second part, the dimensions of the footprints at the bottom and side regions on the aluminum specimen were measured using SEM. The objective of the observation was to characterize the erosion pits with a change in both air pressure p_A and SOD. **Figure 5** compares the images taken at four different levels of air pressure p_A. The images of the free air iPWJ were taken under identical exposure conditions. The photographic images were then processed by applying a contrast threshold to enhance the visibility of the core of the jet and the jet disruption. Here, the jet shape shows a stable widening with increasing SOD in the case of air pressure ranging from the blocked inlet $p_A\,(0)$ to $p_A\,(2) = 2000\,hPa$. At $p_A\,(3) = 3000\,hPa$, the jet shows a one-sided disturbance in width directly after the focus tube. The direction of this irregularity is most likely based on the position of the air inlet.

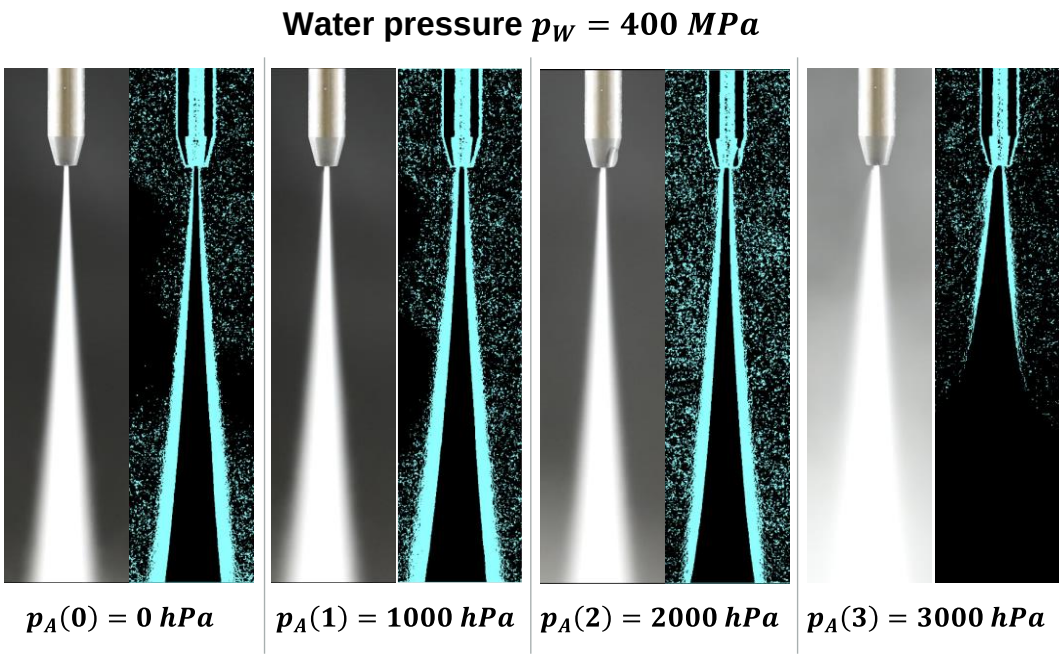

Figure 5. Images of the jet shape for a fixed water pressure level $p_W = 400\ MPa$ over varying air pressure levels p_A. Each photograph was image processed to highlight the jet shape.

Surface morphology SEM analysis

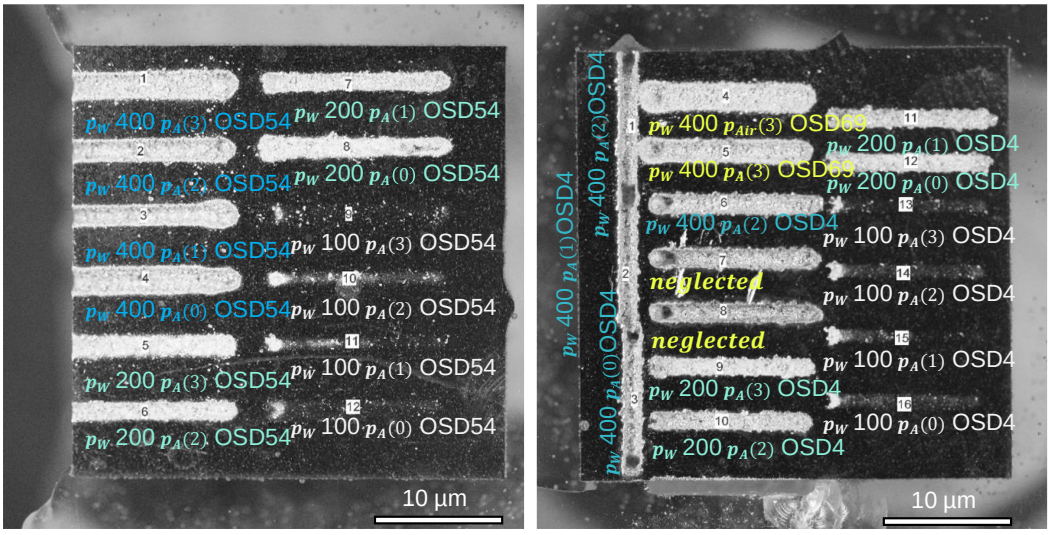

Figure 6. Optical microscopy schematic overview of the samples for SEM

Figure 6 gives a visual overview of the machined specimen. In the naming, the water pressure p_W is noted in MPa, the number after p_A represents the air pressure condition, accompanied by the SOD in mm. A visual comparison revealed significant differences in the groove width in dependence on the air situation. This is especially visible in the case of SOD = 54 mm together with a water pressure p_W = 400 MPa. However, the water pressure of 200 MPa shows a similar trend here.

In **Figure 7**, an overview by SEM imaging is given for a high level of water pressure p_A = 400 MPa. At the low level of SOD = 4 mm, similar groove widths for all four levels of p_A were evident. Opposite to the high level of SOD = 54 mm, a difference was visible in the width of the grooves. The footprint with a blocked abrasive inlet p_A (0) was wider compared to the one created with an open inlet to atmospheric pressure p_A (1). Further, the footprint created with an air pressure p_A (2) = 2000 hPa was similar in appearance to that of atmospheric pressure. However, the centerline of the groove appeared more serrated. An increase in effective jet diameter was enforced at the highest pressure level p_A (3) = 3000 hPa. The center line of the groove created here appeared most uneven and serrated. As an interim conclusion, the observations at a pressure level p_W = 400 MPa revealed, that the jet footprint was at its widest dimension when the air inlet was blocked. For an open inlet, the groove narrowed first until an overpressure of supplied air forced the jet to widen again.

Figure 8 shows an equivalent comparison of grooves created by the low level of water pressure p_W = 200 MPa. Like the previous results, a widening of the jet footprint based on the air pressure level was observed here. Further, the impact of air pressure on the jet's effectiveness was observed very clearly. For both levels of SOD, the jet footprint was most uniform for p_A (1) and p_A (2). Note that the low level of SOD leads to grooves that appear more uniform at p_A (2). In contrast, the high level of SOD revealed a more uniform jet footprint at atmospheric pressure p_A (1). Both the blocked inlet p_A (0) and the pressurized inlet p_A (2) created uneven erosion pits. The high level of SOD supports smaller and more isolated erosion pits at both p_A (0) and p_A (3), respectively.

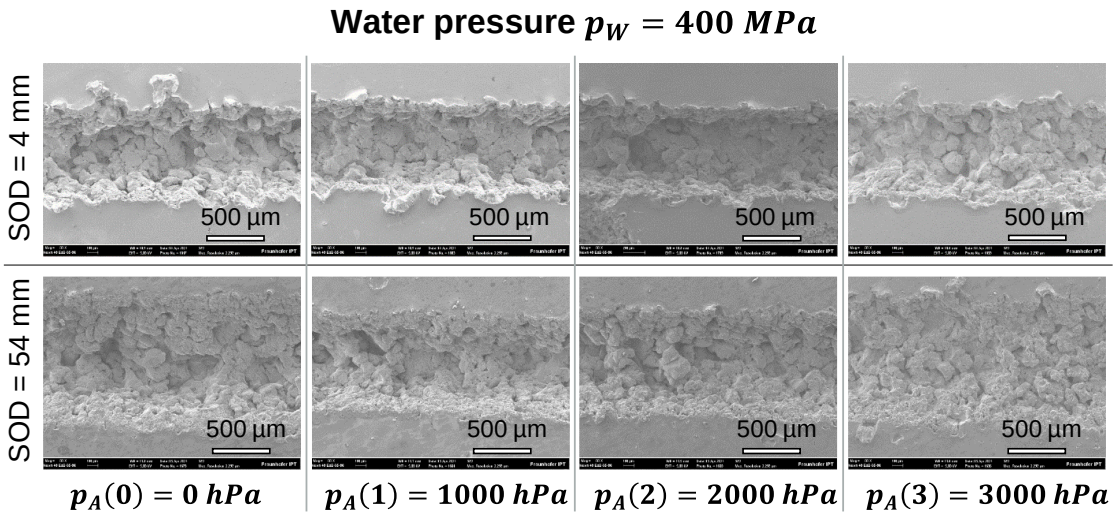

Figure 7. SEM overview of erosion groves machined at a high level of water pressure p_W = 400 MPa: Both levels of SOD at all levels of air pressure p_A

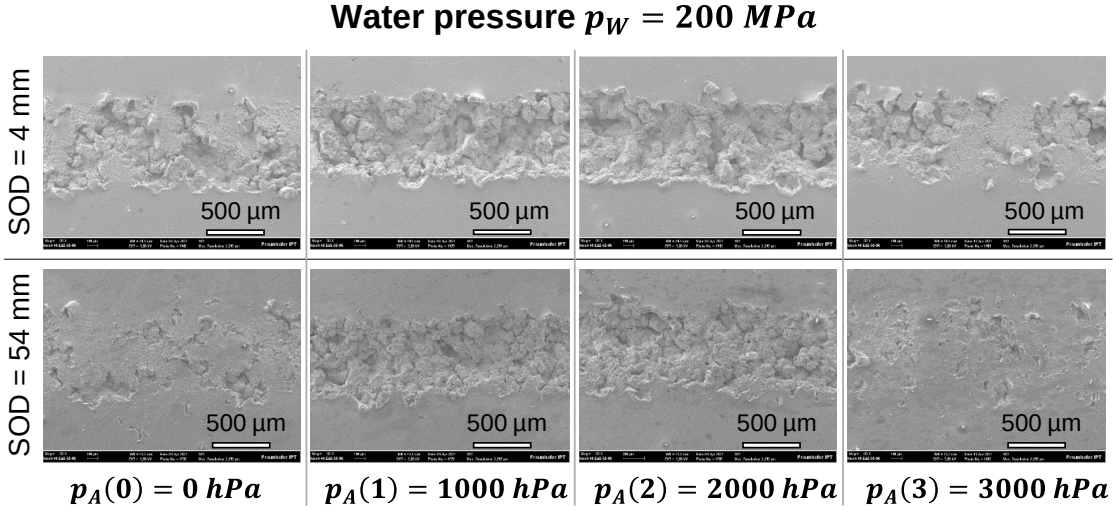

Figure 8. SEM overview of erosion groves machined at the low level of water pressure p_W = 200 MPa: Both levels of SOD at all levels of air pressure p_A

Figure 9 and **Figure 10** compare the detailed images for both levels of SOD at a lower level of water pressure p_W = 200 MPa. Since the changes in jet erosion were more visible on SEM, a detailed overview was given for both the central region and edge region over the levels of air pressure. **Figure 9** shows footprints created at a lower level of SOD = 4 mm while **Figure 10** is related to the high level of SOD = 54 mm, respectively.

In **Figure 9**, the central line at p_A (0) revealed separated pits of deep erosion. The area between the pits was covered with small cavities which can be seen in **Figure 9 a)**. The Pits were characterized by narrow edges and smooth bottoms. A central region of the footprint related to p_A (1) was shown in **Figure 9 b)**. This area consists of a homogenous erosion trench. Compared to pA (2) in **Figure 9 c)**, the area shows more smooth facets. Here, the details also showed several erosion pits of shallow expression and some deeper cavities. It appears that the smooth facets were attributed to both the plastic deformation and the shear of the material caused by lateral outflow. The footprint related to p_A (3) in **Figure 9 d)** shows similar structures to the one corresponding to p_A (0). It features shallow erosion cavities on the surface and marks of

plastic deformation between the larger erosion pits, which were spread across several grains. At the edge region of all footprints, there were small erosion cavities. Both details in **Figure 9 f)** and **g)** show a higher slope of the groove compared to **Figure 9 e)** and **h)**. The edges of the grooves eroded with p_A (2) and p_A (3) in **Figure 9 f)** and **g**) respectively also showed a great number of small but deep cavities. These could be caused by lateral flow and related to the groove gradient. The crack propagating in **Figure 9 e)** shows that the cracks grow on the edges of erosion pits or inside them. **Figure 9 h)** visualizes that constituent particles, which were abundant within the material, appeared to be preferred places for crack initiation and propagation.

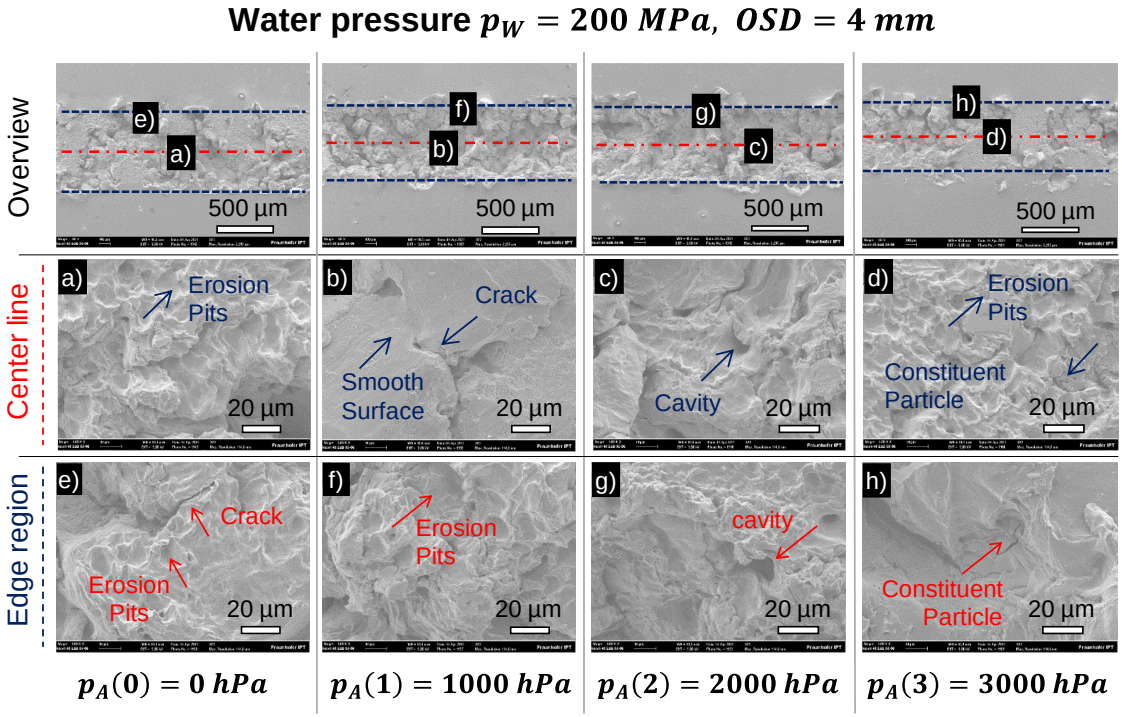

Figure 9. Detailed comparison of footprints machined with the low level of water pressure p_W = 200 MPa at the low level of SOD = 4 mm over variation of the air pressure p_A.

In **Figure 10** a higher level of SOD = 54 mm was displayed, while the basic layout remains identical to the previous Figure 9. In the results, a notable difference was seen in the central region, particularly in the width of pits related to the outer air pressure levels p_A (0) and p_A (3), respectively. In both the detailed **Figure 10 a)** and **d**), the number of shallow erosion cavities increased, but with a decrease in its diameter, most notably seen in **Figure 10 a)**. In comparison, the footprints related to the remaining p_A (1) and p_A (2) were shallower than their counterparts at the lower level of SOD = 4 mm in the previous **Figure 9**. This translates to a less serrated bottom in the region around the center line of both **Figure 10 b)** and **c),** where the bottom of the groove showed a very linear array of pits that were created at p_A (1) in **Figure 10 b**). A similar linear array of pits can be seen on the bottom of the groove related to p_A (2) in **Figure 10 c**). The separated erosion pits at the center line were observable in **Figure 10 d)** at both air pressure levels p_A (0) and p_A (3). A steep drop between the outer wall of the groove and the unaffected surface of the workpiece was recognized. However, the edge region was comparable to the result of SOD = 4 mm. **Figure 10 e)** shows a similar characteristic. It should be mentioned that the edge also showed several cracks near the cavity entrance. For both levels p_A (1) and p_A (2), a steep curve at the edge and considerable pileups were seen in **Figure 10 g)** and **h**), respectively. Pileups were considered in protecting the surface behind them from lateral jetting. **Figure 10 f)** shows

a crack propagating directly from the pile-up. **Figure 10 h)** reveals a high gradient at the groove edges and several deep cavities. The material behind the pileup appeared rather flat and smooth.

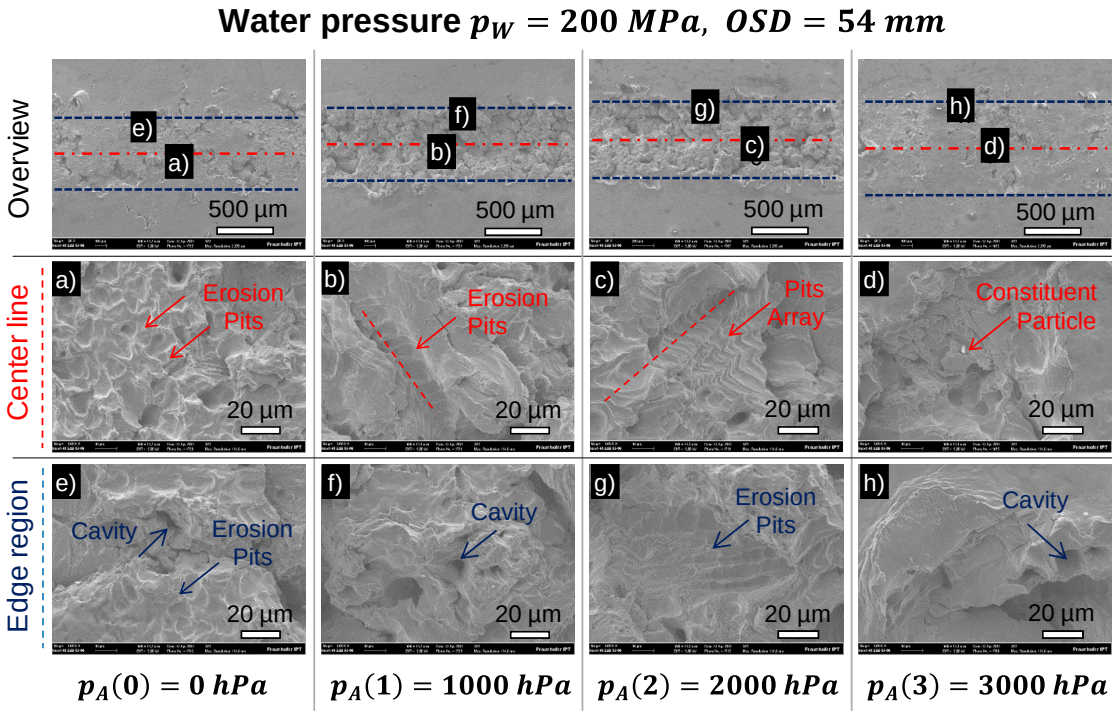

Figure 10. Detailed comparison of footprints machined with the low level of water pressure p_W = 200 MPa at the high level of SOD = 54 mm over variation of the air pressure p_A.

The derived diameter from the jet footprint was plotted in **Figure 11**. Here, the average diameter of the jet tool was obtained from the SEM images by ten individual measurements. For the low level of SOD = 4 mm, a variation in the air pressure revealed only a minor effect on the derived diameter of the jet. More important appeared the influence of the water pressure p_W. The trend was similar, but more pronounced for the high level of SOD = 54 mm. Although the jet diameter could be shifted following the applied levels of air pressure, it was significantly increased at the high level of SOD for both levels of water pressure. There the entrained air helps to disintegrate the jet under free-air conditions, similarly to the creation of cavitation bubbles on the other end. A local minimum of the groove width was found at a moderate air pressure level between p_A (1) and p_A (2). The shape of the trend is convex here. Note that due to the discontinuity of the footprints, some deviations occurred. Notably hard to measure is the location of the groove width at the low level of water pressure p_W = 200 MPa in combination with the outer levels of air pressure p_A (0) and p_A (3), respectively.

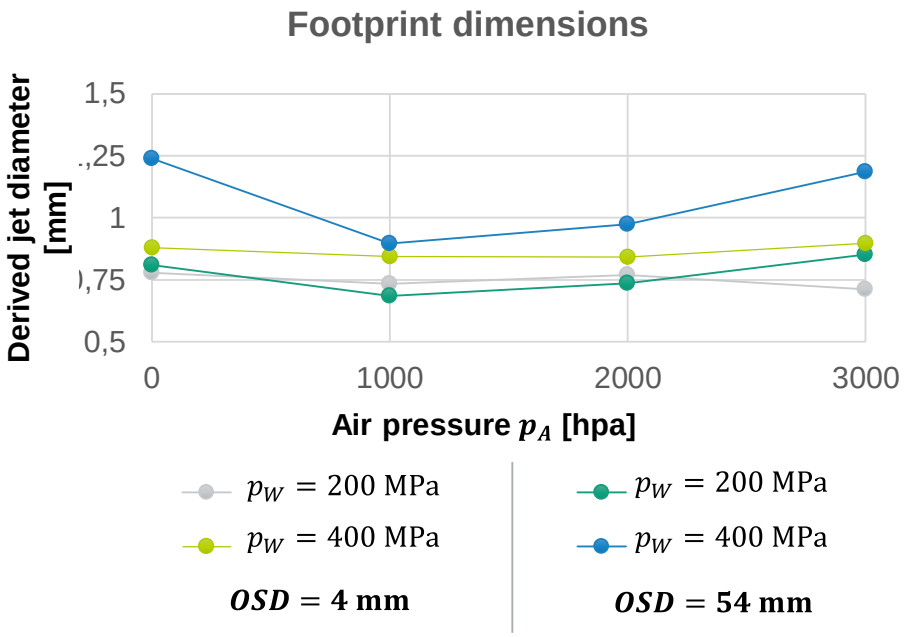

Figure 11. Overview of the footprint dimensions achieved under different levels of pressure conditions for both levels of SOD.

5. Summary and Outlook

In this study, a novel and simple modification of a waterjet tool was practically tested. Here, the fundamentals in jet geometry and erosion characteristics of an injection-type plain waterjet (iPWJ) were investigated for different modifications of the air inlet. From a blocked, up to a pressurized air supply into the iPWJ tool, both its effects on the free jet were visually compared and its footprints on an aluminum alloy were analyzed by SEM methods.

In the continuation of the work by [7] and [12], several conditions of the air inlet were analyzed. Besides the change in the free jet shape, the erosion could be altered. An increase in the erosion depth was seen at the low level of water pressure for both the atmospheric pressure p_A (1) = 1000 hPa and the mildly increased air pressure p_A (2) = 2000 hPa. The effective jet diameter was increased at the outer levels of air pressure, e.g., a blocked inlet p_A (0) or the high level of air pressure p_A (3) = 3000 hPa. While the widening of the free jet was visible at the high level of air pressure, it was not recognized at the blocked inlet. In contrast, the high level of water pressure p_W = 400 MPa revealed a local minimum of the footprint diameter at the air pressure p_A (1) and p_A (2), respectively. On the other hand, the same condition at the low level of water pressure p_W = 200 MPa created the most consistent erosion. It appears that a defined airflow into the iPWJ tool helps to focus the jet and vice versa. Overall, the shape of the free jet correlates well with the findings on the erosion results. The SEM images revealed a decrease in the size of the shallow erosion cavities by the high level of SOD, which was most notable for the outer levels of air pressure. This could be a sign that the jet was losing its coherence due to disintegration under atmospheric drag. However, at the low level of SOD, this could also be caused by changes in the recompression region. A summarization of the findings was given in the following:

- The shape of the free jet correlated well with the dimensions of the footprints.
- Jet stability varied based on the air input. A lowered stability was observed on the footprints at higher SOD.
- The effect of SOD on the size of erosion cavities was observed by SEM analysis of the machined specimen.
- A strong correlation between air pressure and jet diameter was observed for the low level of water pressure. The groove is deep and continuous for medium levels of air pressure. In contrast, both the blocked and highly pressurized conditions revealed isolated erosion pits with small erosion cavities and plastically deformed areas in between.
- The high level of water pressure resulted in pronounced and continuous grooves for all air pressure levels. A notable difference was observed in the apparent increase of groove width for the outer levels of the air pressure, namely a blocked inlet and a highly pressurized condition, respectively.

In the future, experiments should be done to optimize the phase composition of an iPWJ tool for distinctive applications. Here, the extended analysis of high-speed imaging or particle image velocimetry might be helpful. Further, the erosion capabilities of such adapted jet tools should be investigated more in detail to gain an understanding of the jet phase-material interaction. A preliminary evaluation of tool geometry, material removal rate, and surface characteristics on other materials might be necessary for modeling and integration of specific jet tools into computer-aided production. These developments could be promising for future applications of surface treatment with waterjets.

5. Acknowledgments

J. Poloprudsky would like to thank the Ministry of Education, Youth and Sports of the Czech Republic for supporting 3-month research stay at the Fraunhofer Institute for Production Technology IPT through Project No. CZ.02.2.69/0.0/0.0/18_053/0016933.

6. References

[1] Axinte, D.A., Karpuschewski, B., Kong, M.C., Beaucamp, A.T. *et al.*, 2014. High Energy Fluid Jet Machining (HEFJet-Mach): From scientific and technological advances to niche industrial applications, p. 751

[2] Foldyna, 2019. Recent Developments in Pulsating Water Jets. In: Hloch S., Klichová D., Krolczyk G., Chattopadhyaya S., Ruppenthalo-vá L. (eds) Advances in Manufacturing Engineering and Materials. Lecture Notes in Mechanical Engineering. Springer

[3] Jerman M., Zeleňák M. Lebar A. *et al.* (2021) Observation of cryogenically cooled ice particles inside the high-speed water jet. Journal of Materials Processing Technology v. 289

[4] Kong M.C., Axinte D., Voice W., 2011.Challenges in using waterjet machining of NiTi shape memory alloys: An analysis of controlled-depth milling. Journal of Materials Processing Technology

[5] Putz 2018 Putz M., Dix M., Morczinek F., Dittrich M., 2018.Suspension Technology for Abrasive Waterjet (AWJ) Cutting of Ceramics, p. 77

[6] T. Bergs, J.P. Borrmann, M. Schüler, T. Herrig, J.-E. Döring, Editor, 2019. Pure waterjet controlled-depth machining for stripping ceramic thermal barrier coatings on turbine blades. Elsevier B.V.
[7] Osman A.H., Mabrouki T., Théry B., Buisine D., 2004. Experimental analysis of high-speed air-water jet flow in an abrasive water jet mixing tube. Flow Measurement and Instrumentation 15:37–48
[8] Momber A.W, Kovacevic R. 1998. Principles of abrasive water jet machining. Springer.
[9] Momber A.W. 2001. Principles of abrasive water jet machining. Energy transfer during the mixing of air and solid particles into a high-speed waterjet: an impact-force study. Experimental Thermal and Fluid Science 25:31–41
[10] Huang C.Z., Hou R.G., Wang J., et al. 2007. Three-Dimensional Simulation of Liquid-Solid Two-Phase Flow Inside the Abrasive Water Jet Nozzle. KEM 329:329–334
[11] Himmelreich U. 1993. Fluiddynamische Modelluntersuchungen an Wasserabrasivstrahlen ((Fluid-dynamic model investigations on water-abrasive jets)), Ph.D. thesis Hannover: Fortschritt-Berichte VDI, Institut für Werkstoffkunde
[12] Bergs T, Schüler M, Dadgar M, et al. 2020. Investigation of Waterjet Phases on Material Removal Characteristics. Procedia CIRP 95:12–17.
[13] M. Schüler, T. Herrig, T. Bergs. 2022. A study on abrasive waterjet multi-stage machining of ceramics. Procedia CIRP 108:770-775.

7. Nomenclature

PWJ	Plain waterjet
AWJ	Abrasive waterjet
ASJ	Abrasive suspension waterjet
iPWJ	Injection-type plain waterjet
CFD	Computational fluid dynamic
v_{Jet}	Jet velocity
v_F	Feed rate
$\emptyset d_f$	Focus tube diameter
$\emptyset d_w$	Nozzle diameter
MPa	Megapascal as a unit of pressure
hPa	Hektopascal as a unit of pressure
SOD	Standoff distance
SEM	Scanning electron microscopy
EDS	Energy dispersion spectroscopy
SoD	Standoff distance
p_A	Air pressure
p_W	Water pressure